Check for updates

Li₂S/C/SnS₂ composite-based cathode materials for lithium–sulfur batteries

Irshad Mohammad, [iD] * Akzhan Bekzhanov, Yuri Surace [iD] and Damian Cupid

The rapid developments in portable electronic devices, electric vehicles, and smart grids are driving the need for high-energy (>500 Wh kg^{-1}) rechargeable batteries. Lithium–sulfur batteries (Li–S) are of interest due to their high theoretical energy density (2600 Wh kg^{-1} or 2800 Wh L^{-1}), but their commercialisation is restricted by several technical challenges, including the use of a highly reactive lithium metal anode. Using Li₂S as the cathode to couple with Li-free anodes, such as Si and intermetallic alloys, presents a realistic approach to avoiding the safety issues associated with metallic lithium. However, the low electrochemical activity of Li₂S and the shuttling effect of lithium polysulfides (LiPS) prevent the realization of high capacity and good cyclic performance. The usual Li₂S/carbon (C) composite cathode suffers gradual capacity fading over long-term cycling due to irreversible LiPS migration in lithium–sulfur batteries. Although the presence of C in the cathode composite provides a conductive path to utilize the active material, the irreversible migration of LiPS still exists. In this work, we introduce a polar SnS₂ additive in the cathode composite (Li₂S/C) *via* a highly scalable ball milling method to adsorb LiPS. The Li₂S/C/SnS₂ composite acts as a restriction for LiPS by chemisorption and provides a physical barrier to LiPS shuttling. We have synthesized three types of cathode composites with different weight percentages of C and SnS₂ while keeping the amount of Li₂S constant and studied their electrochemical performance in characteristic cells. We found that the Li₂S/C (20%)/SnS₂ (5%) composite shows a high initial capacity of 711 mAh g^{-1} at 0.1C and retains a capacity of around 400 mAh g^{-1} after 100 cycles. In comparison, the Li₂S/C (25%) composite delivered a capacity that was 100 mAh g^{-1} less than that of the Li₂S/C (20%)/SnS₂ (5%) composite after 100 cycles. The approach and design presented in this work could lead to the development of effective shuttle suppression material additives for future Li–S batteries.

Introduction

Although the performance of lithium-ion batteries (LIBs) continues to improve,[1] they are approaching their theoretical specific energy (~ 387 Wh kg^{-1}) using lithium transition metal oxide cathodes and graphite anodes. Furthermore, the limited availability of metals such as Li, Co and Ni leads to a search for alternative battery chemistries which use more abundant materials.[2] Today, research on alternatives to traditional Li-ion cell chemistries is highly motivated by an increasing need for efficient energy storage systems for portable electronic equipment, electric vehicles, and stationary energy storage in large-scale smart grids. Regarding beyond-Li ion technologies, lithium–sulfur batteries (Li–S) have emerged as a potential candidate due to their high energy density, low toxicity, and the abundance of the raw material sulfur.[3,4] However, the

commercialisation of these batteries is hindered by several challenges. These include the low electrical conductivity of sulfur, significant dissolution and diffusion of lithium polysulfides (LiPSs), and the inevitable structural breakdown of the electrode caused by the lithiation process transitioning from the lithiation of sulfur to that of lithium sulfide (Li₂S).[5–9] Despite facing various challenges, recent years have seen significant progress in the development of Li–S cells, and researchers are actively working to address these limitations. Up to now, several strategies have been proposed to enhance the performance of lithium–sulfur systems, including modifications to the sulfur cathode, the design of the electrolyte, stabilization of the lithium anode, and improvement of the separator.[5,10–17]

However, the sulfur cathode typically needs to be paired with lithium–metal anodes, which are subjected to the formation of dendrites that pose serious safety risks.[18–20] Based on the issues above, the implementation of high-performance S-based cathodic materials for lithium–sulfur (Li–S) batteries still remains a great challenge due to the lithium metal anode. In contrast,

AIT Austrian Institute of Technology GmbH, Transport Technologies, Battery Technologies Giefinggasse 2, Vienna, 1210, Austria.
E-mail: irshad.mohammad@ait.ac.at

lithium sulfide (Li_2S) in its fully lithiated state not only mitigates issues associated with electrode microstructure damage from significant volume expansion but can also be matched with lithium-free anodes, such as graphite, silicon, metallic oxides (SnO_2, Fe_2O_3, and MnO_2), phosphorus, and conductive polymers.[21–25] Furthermore, the high melting point of Li_2S gives it excellent thermal stability, enabling the use of various high-temperature (over 500 °C) methods for the effective synthesis of Li_2S-based cathodes, which is not feasible for sulfur due to its relative low melting point, high vapor pressure, and thermal instability. While lithium sulfide holds excellent promise as a high-capacity cathode material for Li–S, it also faces several significant challenges that limit its practical implementation. These challenges include low electronic conductivity, a high initial activation barrier, and polysulfide shuttling.[4,26]

Several approaches have been implemented in the literature to address the shortcomings of the Li_2S cathode. These include mixing Li_2S with conductive carbon materials, like graphene, carbon nanotubes, or carbon black, to form a conductive network to facilitate electron flow.[27–29] Nano-structuring Li_2S into nanosized particles or embedding them in conductive matrices reduces diffusion distances and increases surface contact.[30] A highly conductive carbon network surrounding the Li_2S active material enhances Li_2S utilisation during the electrochemical reaction and helps reduce the initial activation barrier. However, it has been observed that the weak interaction between nonpolar carbon-based materials and polar lithium polysulfides (LiPSs) or Li_2S species results in inadequate confinement. This leads to the easy detachment of LiPSs from the carbon surface, allowing them to diffuse into the electrolyte, which causes capacity decay and poor rate performance. To address this challenge, a straightforward approach would be to trap LiPSs in the cathode by chemical absorption. Some metal sulfides, such as SnS_2, TiS_2, and MoS_2, have been used to weaken the shuttle effect of LiPSs by forming strong bonds.[31] The interaction between metal sulfides and Li_2S generally improves the electrochemical performance through various mechanisms such as catalytic activation of Li_2S conversion and enhanced polysulfide adsorption.[32]

To enhance the electrochemical performance of Li–S batteries, it is essential to combine the benefits of carbon-based additives for increased conductivity and metal sulfides for polysulfide trapping. However, in most studies, the metal sulfide was incorporated into elemental sulfur cathodes. For example, Jun et al. prepared a blended sulfur composite (SnS_2/CNTs/S) for utilizing the advantages of CNTs and SnS_2 to increase the electrode's electronic conductivity and inhibit the polysulfide shuttling effect, respectively.[33] The composite demonstrated promising electrochemical performance, achieving a first discharge capacity of 1308.6 mAh g^{-1} at 0.1C, with a reversible capacity of 1002 mAh g^{-1} after 100 cycles. This work shows that high-performance Li–S cells can be developed by introducing metal sulfides into the elemental sulfur-based cathode. However, knowledge of the influence of metal sulfides on the performance of Li_2S-based cathodes is limited. In this study, we select SnS_2 as the additive for the Li_2S cathode over other metal sulfides due its advantage of being cheap and commercially available. While metal sulfides such as CoS_2, TiS_2, MoS_2, and FeS_2 have demonstrated notable capacity for polysulfide adsorption and redox kinetics. However, they present certain limitations, including high cost and the need for complex surface modification structure. For example, CoS_2 uses a critical raw material and TiS_2 is expensive due to its titanium content, so these were avoided. In case of MoS_2, only edge sites of MoS_2 are catalytic; basal planes are relatively inert. Without defect/phase (1T) engineering, MoS_2 activity can be anisotropic and limited. Whereas FeS_2 may suffer from side reactions and dissolution.[34]

Herein, we report an electrode design consisting of a Li_2S cathode, carbon black, and SnS_2. This design aims to enhance the redox reaction kinetics and suppress polysulfide shuttling by adsorbing larger ions onto SnS_2. To synthesise the electrode, we utilized a high-energy mechanical milling method, which is an effective way to reduce the particle size. We ball-milled commercial Li_2S, carbon black (CB), and SnS_2 in specific molar ratios at high rotation speeds. After ball-milling, the CB particles were embedded in Li_2S particle surfaces, thereby establishing a conductive network for the Li_2S composite, which accelerates electron and ion transfer and enhances the utilization of active materials. We selected SnS_2 as the metal sulfide as it is widely investigated in lithium-ion batteries as the anode material[35–37] and it is a commercially available material. In addition, Sn and S, which are required for the synthesis of SnS_2, are both relatively abundant, low-cost, and environmentally friendly. Our investigations show that the $Li_2S/C/SnS_2$ composite with 5 wt% SnS_2 exhibits promising electrochemical performance: the initial discharge capacity is 711 mAh g^{-1} at 0.1C (1C = 1675 mAh g^{-1}), and a reversible capacity of 403 mAh g^{-1} is achieved after 50 cycles, maintaining this stability up to 100 cycles.

Experimental

Preparation of Li_2S composites

Li_2S (99.9% metal basis), carbon black (CB, super P65), and SnS_2 were acquired from Sigma-Aldrich, IMERYS, and MK nano, respectively. Three types of Li_2S composites were prepared. The first composite was composed of Li_2S and CB in a weight ratio of 75 : 25; the second contained Li_2S, CB, and SnS_2 in a weight ratio of 75 : 20 : 5; and the third composite employed Li_2S, CB, and SnS_2 in a weight ratio of 75 : 12.5 : 12.5. All composites were synthesised using the high-energy ball milling method. Before the milling, all the precursors were dried at 120 °C for 12 hours under vacuum. The ball milling was performed at 600 rpm for 6 hours under an argon atmosphere using a planetary-type mill (FRITSCH Pulverisette 6). To achieve these conditions, the ball milling vessel was loaded with Li_2S, CB, SnS_2 and the balls in an argon-filled glove box and closed using a mechanical clamp with a Teflon ring between the lid and the jar. The ball milling jar with the mechanical clamp was loaded into the planetary-type mill, thereby ensuring an
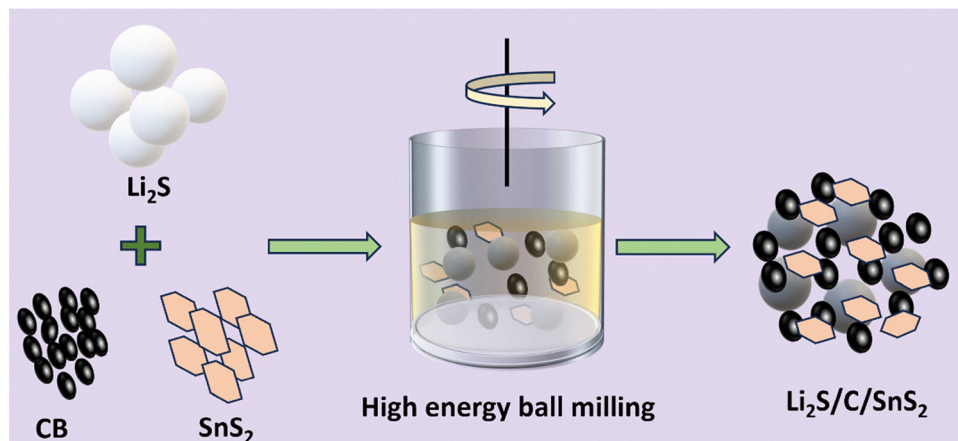
Fig. 1 Schematic illustration of the preparation of Li$_2$S/C/SnS$_2$ composites.

argon-atmosphere during milling. The ball-to-powder weight ratio was maintained at 16:1. Zirconia oxide jars (volume, 80 mL) and 10 balls (diameter, 10 mm) were used as the milling media. The composite synthesis scheme is described in Fig. 1.

Physico-chemical characterisation

Phase identification was carried out by powder X-ray diffraction (PXRD) using an X'Pert Pro diffractometer (Malvern/Panalytical) equipped with Cu Kα radiation (λ = 1.54060 Å). Samples for XRD were prepared in an Ar-filled glovebox and sealed in a sample holder with a polymer cap. The PXRD patterns were acquired between 10 and 80° (2θ) with a scan speed of 0.01061° s^{-1}. The specimen displacement, peak deconvolution, and unit cell parameters were refined by Rietveld analysis within the Highscore Plus software package. Zetium (Panalytical, Netherlands) wavelength dispersive X-ray fluorescence (WDXRF) was utilized for the elemental analysis of the samples. The samples were irradiated using X-ray emissions from a Rhodium (Rh) tube, which operated at a maximum power of 4000 W, a maximum voltage of 60 kV, and a maximum current of 125 mA. The measurement was conducted using a fine collimator, an analyzing crystal of LiF200 (0.124 Å), and a scintillation counter as the detector. For the data analysis, SuperQ 6.0 software was used. For all elements evaluated in this study, only the electronic transition, Kα, was considered. All the sample analyses were done under an inert atmosphere. The samples were airtight using proline films on the front and back of the electrode. A scanning electron microscope (SEM, Supra 40, Carl Zeiss AG, Oberkochen, Germany) was used to investigate the morphology of Li$_2$S composite powders. The elemental distribution was analysed by energy dispersive X-ray spectroscopy (EDX, EDAX Inc., Mahwah, NJ, USA).

Electrode preparation

Due to the air- and moisture-sensitive nature of Li$_2$S, slurry preparation and coating of the Li$_2$S/C/SnS$_2$ composites onto the current collector were performed in an argon-filled glovebox, in which the moisture and oxygen contents were kept below 0.1 ppm. In the first step, a 3 wt% SBR (poly(styrene-co-butadiene) rubber, Sigma-Aldrich) solution was prepared in a toluene solvent. In the next step, the Li$_2$S, SnS$_2$ and CB additive were mixed together using an agate mortar and then added to the prepared 3% SBR/toluene solution, followed by vigorous magnetic stirring for two hours. After this, the homogeneous slurry was coated on 15 μm thick carbon-coated aluminium foil with a doctor blade with a gap thickness of 120 μm and then dried at 120 °C for 12 h. Subsequently, the dried electrode was cut into circular discs with a diameter of 15 mm. The mass loading of the active materials on the current collector was around 1 mg cm^{-2}. The actual Li$_2$S sulfur content for each electrode was 60%.

Electrochemical testing

LiNO$_3$ (99.99%, anhydrous) and LiTFSI (99.9%), which were used for the electrolyte formulation, were purchased from Sigma-Aldrich and Solvionic, respectively. The electrolyte contained 1 M lithium bis(tri-fuoromethanesulfonyl) imide (LiTFSI) salt in the 1,2-dimethoxyethane (DME, Sigma Aldrich, anhydrous, 99.5%) and 1,3-dioxolane (DOL, Sigma Aldrich, anhydrous, 99.8%) solvents (1:1 v/v) with the LiNO$_3$ additive (1 wt%). Before preparing electrolytes, solvents were dried by placing 4 Å molecular sieves (Sigma Aldrich, 8–12 mesh) into the solvent bottles at around a third of the solvent volume in order to dry for at least 3 days. Also, LiTFSI and LiNO$_3$ were dried at 120 °C and 80 °C for 2 days in Buchi under vacuum, respectively. Finally, the appropriate amounts of LiTFSI and LiNO$_3$ salts were dissolved in the solvent mixture (DME and DOL) and stirred overnight at room temperature. Li$_2$S/C/SnS$_2$ composite cathodes were coupled against lithium metal anodes and tested in CR2032 coin cells, which were assembled in the Ar filled glove box. A Celgard separator soaked with the electrolyte was sandwiched between the cathode and anode discs in the cell. All charge–discharge processes were started with a slow charge rate of 0.05C to 3.5 V and then cycled between 1.7 and 2.8 V vs. Li$^+$/Li at the desired C-rate using an Arbin battery tester. The theoretical capacities of the three composite-based cells ranged from 2 to 2.5 mAh. Electrochemical impedance spectroscopy (EIS) was performed using a

biologic instrument in the frequency range of 1 MHz to 0.1 Hz and a voltage amplitude of 5 mV. The cyclic voltammetry (CV) data were also acquired using the biologic cycler. Data were obtained from the open circuit voltage to 3.8 V for the first anodic scan and between 1.5 and 3.0 V vs. Li^+/Li for the remaining scans at different scan rates. The amount of electrolyte used in each cell was calculated based on an E/S ratio of 12 ($\mu L\ mg^{-1}$). The specific capacity of all cells is calculated based on the mass of Li_2S in the $Li_2S/C/SnS_2$ composite.

Result and discussion

Preparation and characterisation of Li₂S composites

Three types of Li_2S electrode composites with different weight percentages of carbon black and SnS_2 additives were prepared. The first one (Li_2S/C) consists of Li_2S and carbon black in a 75 to 25 wt% ratio, the second one ($Li_2S/C/SnS_2$ (5%)) contains Li_2S, carbon black (C), and SnS_2 in a ratio of 75, 20, and 5 wt%, and the third composite is $Li_2S/C/SnS_2$ (12.5%), which constitutes Li_2S, carbon black, and SnS_2 in 75, 12.5 and 12.5 wt% ratios. The details of the percentage of the constituents in the three composites are given in Table S1.

The Li_2S electrode composites were prepared by high-energy ball milling, and their structural characterisation was performed using XRD, XRF, and SEM techniques. The milling media and parameters are detailed in the Experimental section. Fig. 2(a) shows the XRD patterns of the composites and compared with the original XRD pattern of Li_2S. In the XRD pattern, all the samples exhibited the same peaks, despite their differing constituents in the composite. The diffraction peaks are well matched to the Li_2S phase with a cubic structure indexed to the $Fm\bar{3}m$ space group. The peak broadening and the smaller crystallite size are typical for high-energy ball-milled samples.[30,38] Ball milling involves high-energy impacts that repeatedly fracture particles, resulting in smaller crystallite sizes. Interestingly, no peaks corresponding to carbon black and SnS_2 phases were observed for samples 2 and 3 (Fig. 2a, middle and top layers). High-energy ball milling was employed to mix and decrease the particle size of Li_2S, C, and SnS_2 materials. This intense milling process breaks particles into very small sizes, such as nanocrystals, or even creates amorphous materials. Carbon black and layered SnS_2 are especially prone to becoming amorphous during milling. As a result, the structure ends up being amorphous, nanocrystalline, or
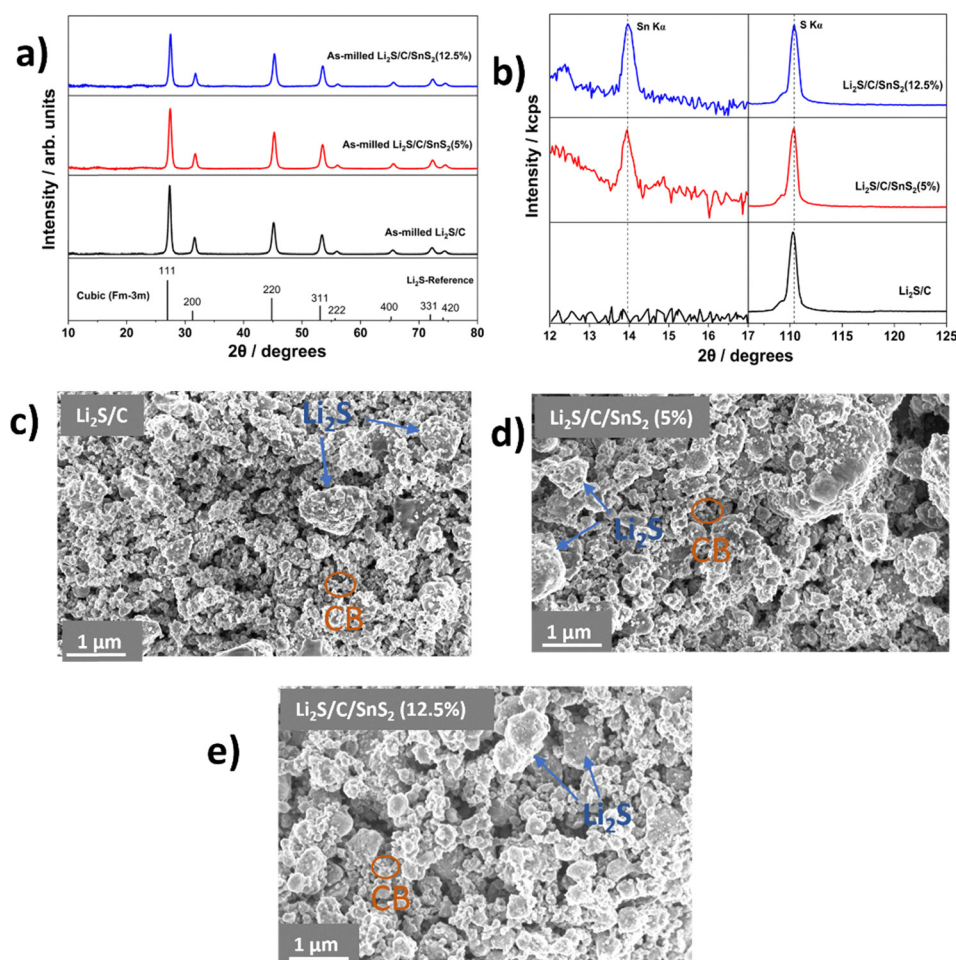

Fig. 2 (a) XRD patterns and (b) XRF spectra of Li₂S composites. SEM images of Li₂S composites (c) without SnS2, (d) with SnS₂ (5%), and (e) with SnS₂ (12.5%) additives.

Table 1 Results of Rietveld refinement for as ball-milled Li_2S composites

Composite	Cell parameter of Li_2S (Å) $a = b = c$	Crystallite size of Li_2S (nm)	Crystallite (rms) strain of Li_2S (%)
Li_2S/C	5.7195	21.0	0.338
$Li_2S/C/SnS_2$ (5%)	5.7254	16.9	0.262
$Li_2S/C/SnS_2$ (12.5%)	5.7201	16.7	0.164

partially reacted and integrated into an amorphous matrix, with only crystalline Li_2S remaining detectable by XRD. Rietveld refinement was performed on the patterns to determine the cell parameters and crystallite size values (Fig. S1 and Table 1). The unit cell parameter values were almost identical for each composite around 5.72 Å. However, the calculated average crystallite size values for Li_2S in the Li_2S/C, $Li_2S/C/SnS_2$ (5%), and $Li_2S/C/SnS_2$ (12.5%) composites were 21.0, 16.9, and 16.7 nm, respectively, which is smaller than the as-received Li_2S (1 μm). Interestingly, the crystallite size of the Li_2S/C composite with SnS_2 is slightly higher than that of other composites with the SnS_2 additive. This means that adding SnS_2 to the composite helps decrease the crystallite size of Li_2S during high-energy ball milling.

Wavelength dispersive X-ray fluorescence (WDXRF) analysis was performed on all three Li_2S composites for the qualitative analysis of the elements present in the samples, as shown in Fig. 2b. In the low 2θ range from 12 to 17, both composites $Li_2S/C/SnS_2$ (5%) and $Li_2S/C/SnS_2$ (12.5%) displayed a peak at $14°$ (2θ) corresponding to the Sn Kα line, suggesting the presence of SnS_2 in the composites. As expected, no peak corresponding to the Sn Kα line for Li_2S/C was observed between $12°$ and $17°$. At higher 2θ values, all the composites exhibited an S Kα line at $110°$, which may be associated with Li_2S and SnS_2, respectively.

The surface morphology of the Li_2S composites was examined using scanning electron microscopy (SEM), as shown in Fig. 2c–e. The Li_2S/C and $Li_2S/C/SnS_2$ (5% or 12.5%) composites displayed similar morphologies and homogeneous particle distributions of Li_2S, CB, and the SnS_2 additive. The particle sized between 300 nm and 1 μm is identified as Li_2S, indicated by the blue arrow (Fig. 2c–e). Smaller particles, around 50 to 100 nm, correspond to carbon black, represented by circles (Fig. 2c–e). Unfortunately, it was difficult to visualize the plate-like SnS_2 in the SEM images, possibly because they were crushed into smaller piece particles by high-energy ball milling. EDX mapping analysis was performed on the surfaces of the composites to monitor the distribution of Li_2S, carbon black, and SnS_2. Fig. S2(a–d) shows the EDX mapping images for the $Li_2S/C/SnS_2$ (5%) composite. The elements C, S, and Sn were found to be homogeneously distributed in the composite.

Electrochemical testing of the Li_2S composite electrodes

The charge profiles of the activation process of the cells using ball-milled Li_2S composites as well as pure Li_2S electrodes are shown in Fig. 3a, where the cells were charged from the open-circuit voltage to 3.5 V at a current density of 0.05C. The Li_2S electrodes were prepared using the same procedures as the composite electrodes. However, high-energy ball milling of Li_2S was not performed, as the aim was to investigate the electrochemical performance of as-received Li_2S without any pre-processing. In these experiments, a high upper cutoff voltage of 3.5 V was adopted to overcome the kinetic barrier of phase nucleation from Li_2S to LiPSs, which is referred to the initial activation process of Li_2S cathodes.[22] It is observed that, at the start of the charge process, all the Li_2S composites exhibit an initial increase in potential to approximately 2.45 V, accompanied by a charge plateau at around 2.38 V vs. Li/Li$^+$, with negligible relative activation potential differences of around 0.1 V among the three composites. In contrast, the pure Li_2S electrode shows an initial potential increase up to ca. 3.4 V, followed by a gradually increasing plateau starting from ca. 3.1 V, corresponding to an increase in plateau voltage of 0.72 V in comparison to Li_2S composites. The extremely small activation barrier of the Li_2S composites may be attributed to the smaller-sized ball-milled Li_2S particles, which are well embedded in the carbon black and Li_2S additive matrix and their intimate contact with the carbon matrix. On the other hand, the high activation barrier and charge voltage plateau of pure Li_2S (as commercially received) is due to its big particle size (ranging in micrometres). The SEM images of the received Li_2S show that the particles are of micrometric size, as illustrated in Fig. S3. In general, larger Li_2S particles have a lower surface area, resulting in fewer electrochemically active sites for Li_2S oxidation, which leads to slower reaction kinetics and increased polarization. The high energy ball milling method not only decreases the particle size of Li_2S but also helps in uniformly distributing the active material, carbon and additives. This result is in good agreement with previous findings where Li_2S and carbon composites were prepared and investigated.[38,39]

Fig. 3b–d illustrates the charge–discharge profiles of the Li_2S-based composites over the first five cycles at 0.1C. Cell cycling was performed between the operating voltage limits of 1.7 and 2.8 V vs. Li$^+$/Li, respectively. The charge curves for each Li–S composite show two plateaus, a long plateau at 2.3 V followed by a relatively short plateau that slightly increases from ca. 2.3 V to 2.38 V, consistent with previous reports related to Li_2S and carbon composites. The first plateau relates to the delithiation of Li_2S to Li_2S_x ($3 \leq x \leq 8$), whereas the second one corresponds to the further delithiation of Li_2S_x ($3 \leq x \leq 8$) to elemental S_8. Similarly, two discharge plateaus were observed for all the composite electrodes. The sloping plateau in the comparatively high potential range between 2.5 V and 2.3 V corresponds to the lithiation of S_8 to Li_2S_x, and the latter in the comparatively low potential range corresponds to the further reduction of Li_2S_x to Li_2S. The latter process is the main one, generating more capacity than the first discharge process at higher potential. All the Li–S composite electrodes show similar voltage profile behaviours, which correspond only to the electrochemical activity of Li_2S. This is confirmed by the charge–discharge profiles of the pure Li_2S electrodes, which are shown in Fig. 3(e). In the Li_2S composites with SnS_2, no extra plateau related to the lithiation of SnS_2 was observed. Therefore, based
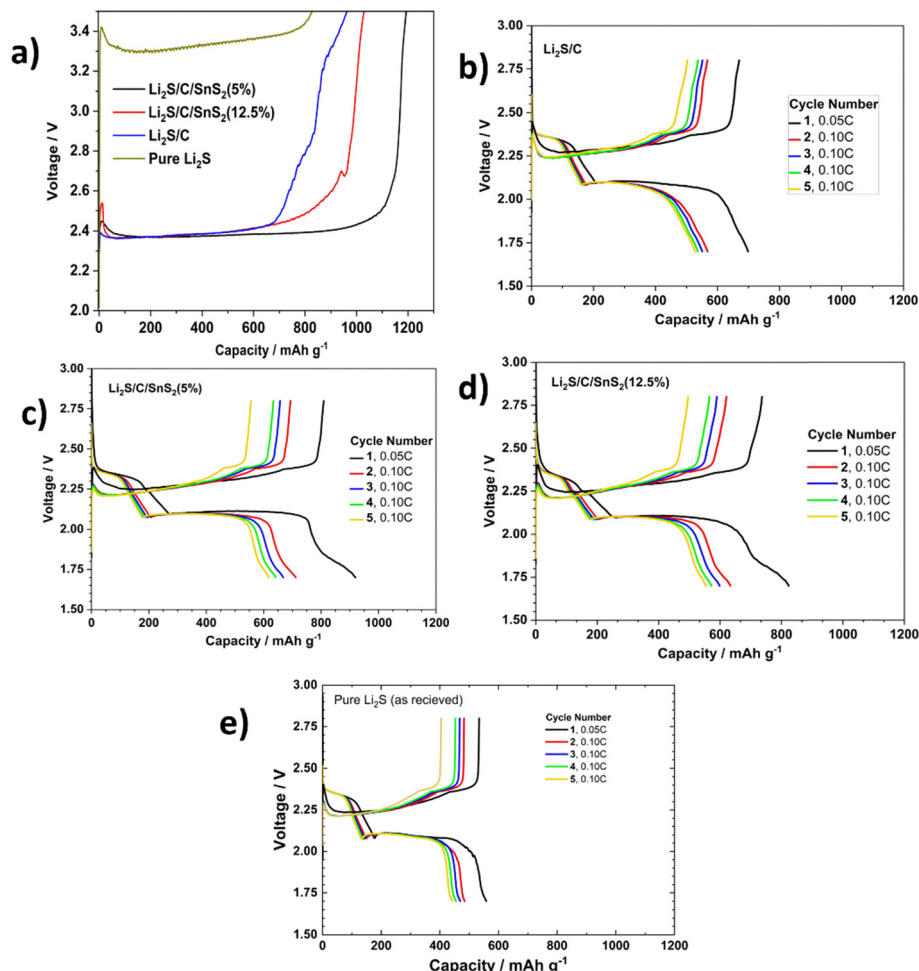
Fig. 3 (a) Charge profiles of the activation process of the as-ball milled Li_2S composites and the as-received Li_2S. The first five galvanostatic charge–discharge curves of Li_2S electrodes after an initial activation: (b) Li_2S/C, (c) $Li_2S/C/SnS_2$ (5%), (d) $Li_2S/C/SnS_2$ (12.5%), and (e) pure Li_2S.

on charge–discharge profiles, the mechanism of the delithiation and lithiation processes of Li_2S may be the same for all types of electrodes. Nonetheless, the capacity in each cycle was greater for the $Li_2S/C/SnS_2$ (5%) composite compared to the other composites.

Further cycling performance and coulombic efficiency of the Li_2S composite electrodes are displayed in Fig. 4a. $Li_2S/C/SnS_2$ (5%) exhibits a high first discharge capacity of 712 mAh g^{-1} and retains a discharge capacity of 391 mAh g^{-1} at 0.1C after 100 cycles, corresponding to a capacity retention of 55%. In comparison, the initial capacities of Li_2S/C and $Li_2S/C/SnS_2$ (12.5%) are 568 and 625 mAh g^{-1}, and capacities of 320 and 277 mAh g^{-1} are recorded after 100 cycles, corresponding to capacity retentions of 56% and 44%, respectively. The initial coulombic efficiencies of the Li_2S composites are 84%, 85%, and 87%, for Li_2S/C, $Li_2S/C/SnS_2$ (5%), and $Li_2S/C/SnS_2$ (12.5%), respectively, which do not seem high. The low initial coulombic efficiency is presumed to be a result of the polysulfides generated from the weakly trapped Li_2S near the surface of Li_2S/C, which easily dissolve in the electrolyte in the initial cycle. However, the coulombic efficiency increases to 96–98% and

tends to be stable when the weakly trapped Li_2S is consumed in the initial several cycles. In particular, for $Li_2S/C/SnS_2$ (5%), only a few cycles are needed for reaching a high stable value of 99%, as seen from Fig. 4a. The increase of coulombic efficiency after the initial several cycles is commonly found in other $Li_2S/$ C systems.[27,38] Additionally, the cycling performance of the pure Li_2S electrode was conducted and is shown in Fig. S4. The initial and 100th cycle capacities of the pure Li_2S were approximately 560 and 200 mAh g^{-1}, respectively. Although the initial capacity of the pure Li_2S cathode is similar to that of the $Li_2S/C/SnS_2$ (12.5%) composite, this electrode exhibits significant capacity decay, dropping to 200 mAh g^{-1} after 100 cycles. This means that SnS_2 works by inhibiting the shuttle effect of lithium polysulfides and enhances electrochemical performance through the adsorption of lithium polysulfides to prevent the loss of the active material.

Additionally, the voltage polarization of both Li_2S and $Li_2S/$ C/SnS_2 (5%) composite cells was calculated and compared, as shown in Fig. S5. The Li_2S cell exhibited a voltage polarization of 0.2 V, while the $Li_2S/C/SnS_2$ (5%) cell showed a lower polarization of 0.16 V. This indicates that adding SnS_2 to the
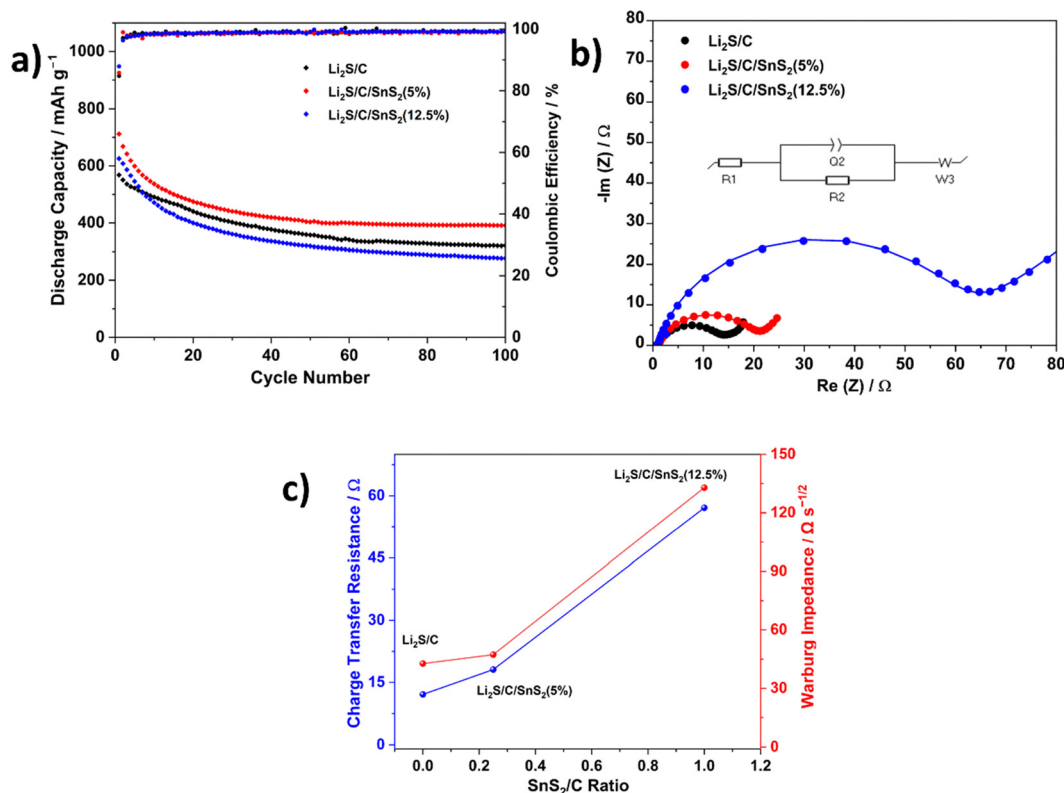
Fig. 4 (a) Cycling performance (including coulombic efficiency) at a current rate of C/10 and (b) Nyquist plots before cycling for of Li$_2$S/C, Li$_2$S/C/SnS$_2$ (5%), and Li$_2$S/C/SnS$_2$ (12.5%) electrodes. (c) Linear plot of charge-transfer resistance and Warburg impedance against the SnS$_2$/C content in the composites.

composite helps facilitate the redox process, thereby reducing the voltage gap between the charge and discharge plateaus. In summary, SnS$_2$ in the Li$_2$S/C/SnS$_2$ composite serves a dual purpose by improving redox kinetics and polysulfide adsorption. Its polar surface interacts strongly with lithium polysulfides, effectively immobilizing them and mitigating the shuttle effect that often leads to capacity fade in Li–S batteries. Additionally, SnS$_2$ acts as an electrocatalyst, enhancing fast redox reactions by lowering the energy barrier for converting soluble polysulfides into insoluble forms Li$_2$S/Li$_2$S$_2$.

The electrochemical reaction kinetics of the Li$_2$S composites were further investigated by electrochemical impedance spectroscopy (EIS), which was performed on the electrodes in the fresh state. Complex impedance spectra obtained at 25 °C for Li$_2$S/C, Li$_2$S/C/SnS$_2$ (5%), and Li$_2$S/C/SnS$_2$ (12.5%) electrode based cells are shown in Fig. 4b. In addition, an equivalent circuit (inset in Fig. 4b) was used to fit the impedance data, which are composed of two resistors (R1 and R2), a constant phase element (Q2), and a Warburg element (W3). Referring to Fig. 4b, R1 is the bulk resistance of the cell, which represents the combined resistances of the electrolyte, separator, and electrodes. R2 and Q2 are the charge-transfer resistance and related constant phase element, respectively, while W3 is the Warburg impedance related to the diffusion of ions in the electrode material. As it can be seen in the figure, all the spectra consist of a single depressed semicircle at high frequencies and

a tilted straight line at low frequencies. The semicircle corresponds to the charge transfer resistance, while the straight line is related to Warburg impedance. The fitting curves (shown as solid lines) and the measured plots (symbols) fit quite well for all spectra (Fig. 4b). The parameters of the equivalent circuit after fitting all spectra are presented in Table S2. All the electrodes exhibited the same electrolyte resistance (R 1), which was approximately 1 Ω, indicating high electrolyte conductivity. The Li$_2$S/C/SnS$_2$ (5%) and Li$_2$S/C electrodes show low charge transfer resistance values of 21 and 13 Ω, respectively, indicating the faster charge transfer and higher electron conductivity. However, the Li$_2$S/C/SnS$_2$ (12.5%) electrode exhibits the highest charge transfer resistance value of 57 Ω among the electrodes, which might be due to its low conductivity originating from the higher content of SnS$_2$ and the lower amount of C in that composite formulation compared to the other composites. The EIS data conclusively show that increasing the carbon content[37,38] also decreases the SnS$_2$ content, improving the charge transfer resistance of the electrodes, as can be seen in Fig. 4c and d. Similar to charge transfer resistance, Warburg impedance also follows a linear trend against the SnS$_2$/C content. This means that resistance to ion movement within the electrode increases as the SnS$_2$/C content increases (Fig. 4d).

Since the Li$_2$S/C/SnS$_2$ (5%) composite cathode exhibited the best cycling performance, it was selected for further
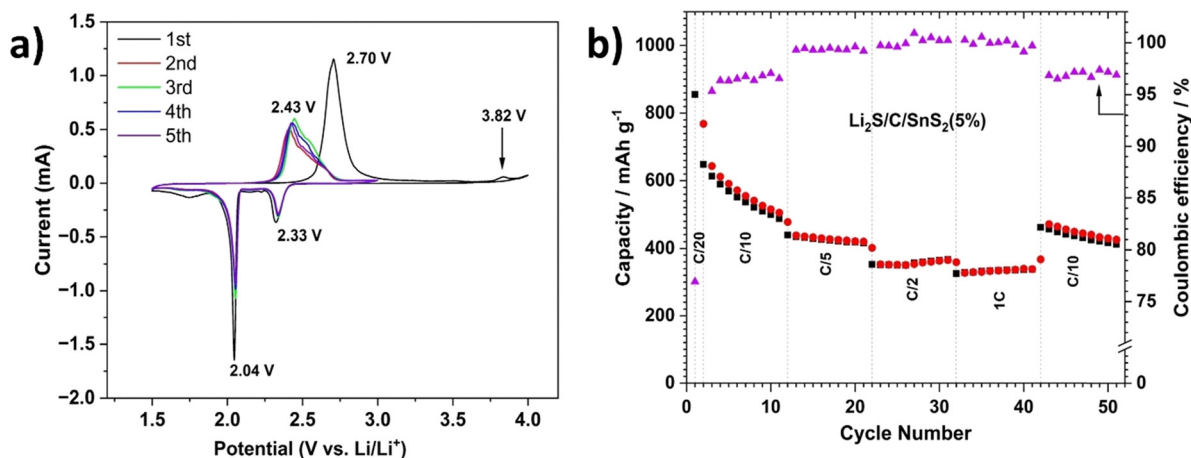
Fig. 5 (a) CV profiles of $Li_2S/C/SnS_2$ (5%) electrodes obtained at a scan rate of 0.1 mV s^{-1}. (b) Rate performance of $Li_2S/C/SnS_2$ (5%) electrodes at a current rate range of C/10 to 1C.

electrochemical investigations such as cyclic voltammetry (CV), rate capability and impedance spectroscopy. The CV curves of the $Li_2S/C/SnS_2$ (5%) cathode for the first five cycles at a scan rate of 0.1 mV s^{-1} are displayed in Fig. 5a. A very typical CV behaviour like the Li_2S cathode was observed consisting of one anodic peak and two cathodic peaks. In the first charge cycle, the anodic peak located at 2.70 V may be attributed to the oxidation of Li_2S to elemental sulfur, matching with the activation charge process. In subsequent cycles, the anode peak shifted to lower potentials, due to the improvement of reaction kinetics of Li_2S after activation and during cycling. In the cathodic sweep, the first peak centred at 2.33 V corresponds to the conversion of sulfur to polysulfides. The second cathodic peak was observed at a relatively low potential of 2.04 V and is attributed to the reduction of polysulfides to Li_2S_2 and/or further reduction to Li_2S. The cathodic peak in the low potential range shows much higher intensity than that in the high potential range, indicating that more capacity is generated in the low potential range. These findings are very much in agreement with the charge–discharge data of Li_2S-based Li–S cells for the first five cycles as shown in Fig. 3.

To further evaluate the electrode kinetics and stability of the $Li_2S/C/SnS_2$ (5%) cathode, the coin cell was subject to cycling at different C-rates and is shown in Fig. 5b. As indicated in the rate capability plot, when the rate was increased from 0.1C to 0.2C, the capacity decreased from 613 to 438 mAh g^{-1}. The capacity decreased again from 419 to 352 mAh g^{-1} when the rate increased from 0.2C to 0.5C. It is important to note that the battery still delivered a high capacity of 325 mAh g^{-1} even at a 1C rate. After 40 cycles with different rates, the C rate was switched back to 0.1C and the capacity recovered to 462 mAh g^{-1}, which is slightly higher than the capacity delivered by the cell if it would be subject to 40 cycles at a 0.2C rate continuously. These results illustrate the possibilities of fast kinetic reactions and the highly robust ability of the Li_2S material with carbon and the SnS_2 additive. $Li_2S/C/SnS_2$ (5%) not only displays a higher reversible capacity, but also owns a longer cycle life compared to other composites. To further

validate the material's practicality and stability, the rate capability test at even higher C rates, from 1C to 5C, was performed on the $Li_2S/C/SnS_2$ (5%) based cell, as shown in Fig. S6. As seen from the cycling graph, the cell exhibited reasonable capacities and stability even at high C rates. At 5C, the discharge capacity was approximately 228 mAh g^{-1}, demonstrating high rate capability and stable performance.

EIS measurements were performed before and after 200 cycles to understand the high capacity and cycling stability of the Li–S cell with the $Li_2S/C/SnS_2$ (5%) cathode. The cycling performance of $Li_2S/C/SnS_2$ (5%) and Li_2S/C after 200 cycles is shown in Fig. S7, which was cycled following an EIS measurement at OCV. As observed in the figure, the capacity was slightly lower for both the $Li_2S/C/SnS_2$ (5%) and Li_2S/C electrodes, possibly due to the effect of the EIS measurement as it was observed in an earlier work.[40] However, the cells still demonstrated stable cycling performance on long cyling. In Fig. 6a, the Nyquist plots of the cell were fabricated using the $Li_2S/C/SnS_2$ (5%) cathode. An equivalent circuit was used to fit both impedance spectra, as shown in Fig. 6b. The equivalent circuits for fitting the Nyquist plots, along with the corresponding circuit parameter values, are presented in Table S3. Before cycling (Fig. 6a), the impedance spectra show one semicircle and a tilted straight line at high and low frequencies, respectively. The semicircle corresponds to the charge transfer process whereas the straight line is related to the lithium-ion diffusion process.[13,41] After testing for 200 cycles (Fig. 6a), the impedance spectrum consists of two semicircles at high and medium frequencies, attributed to interfacial and charge transfer resistances, and one straight line at a low frequency corresponding to ionic diffusion within the active material. It is worth noting that no additional semicircle was obtained which could have corresponded to the presence of an Li_2S_2/Li_2S film. This indicates that the reduced shuttling of higher-order polysulfides resulted in less formation of the solid Li_2S film at the anode, leading to the associated decrease in resistance. Before cycling, the cell exhibits an electrolyte resistance of approximately 1 Ω, which increases slightly to 3 Ω after cycling.
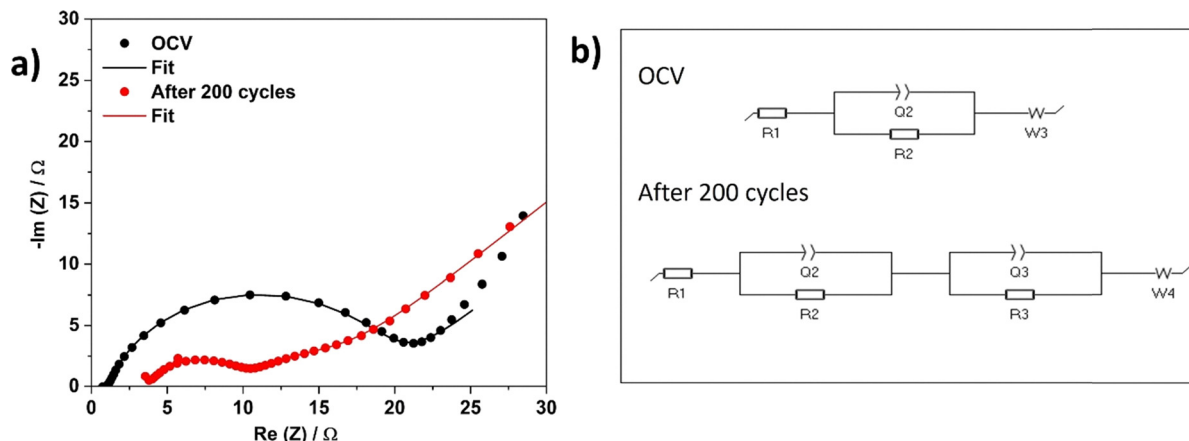
Fig. 6 (a) Nyquist plots of the Li−S cell employing the $Li_2S/C/SnS_2$ (5%) cathode before and after cycling. (b) Equivalent circuits for fitting the impedance spectra at OCV and afterward cycling. For OCV equivalent circuit: R1 = electrolyte resistance, R2 and Q2 are resistance and constant phase elements for the charge-transfer process, and W3 is Warburg-related Li^+ diffusion into the electrode. For the after cycling equivalent circuit: R1 is electrolyte resistance, R2 and Q2 are related to the solid electrolyte interphases, R3 and Q3 are associated with the charge-transfer process, and W4 is connected to lithium-ion diffusion into the electrode.

Therefore, the electrolyte does not densify with polysulfide dissolution and its conductivity remains high. A charge transfer resistance (R2) of 21 Ω is observed for the cell before cycling, which is related to the native passivation of the electrode. After cycling, the charge transfer resistance (R3) value decreases to 4.4 Ω. This significant decrease upon cycling reveals an increase in electrochemical activity of the Li_2S material. After cycling, the cell shows the SEI resistance (4.2 Ω) in the range of the electrolyte resistance (3 Ω), representing the formation of stable and Li^+ ion conductive SEI. These above results further demonstrate that the synergy created inside the Li_2S composite using the SnS_2 and carbon additives resulting in fast reaction kinetics, increase in utilisation of the active material, and reduction of polysulfide shuttling, attesting the excellent electrochemical performance.

To confirm the reduction in polysulfide shuttling due to their adsorption by composites, a Li_2S_6 solution was prepared by a typical combination reaction of sulfur and Li_2S in a mixture solution of DOL and DME (1 : 1 by volume) at a molar ratio of 5 : 1. After stirring at 80 °C for 10 h in an Ar-filled glovebox, the 0.0025 M Li_2S_6 solution was used for the LiPS adsorption experiment. 10 mg of the $Li_2S/C/SnS_2$ (5%) composite was added into 5 ml of this solution, and the colour of the solution was observed over a period of *x* hours. The results of these experiments are presented in Fig. 7 and compared to those of the solution without any composite material. The optical photographs show that the composite is indeed able to absorb the Li_2S_6, thereby changing the colour from dark yellow to light green.

Based on the above electrochemical performance of the Li_2S-based composites and the polysulfide absorption test, the incorporation of carbon and SnS_2 into the Li_2S-based composites enhances the performance of the cathode material by improving conductivity, stabilizing Li_2S, and mitigating

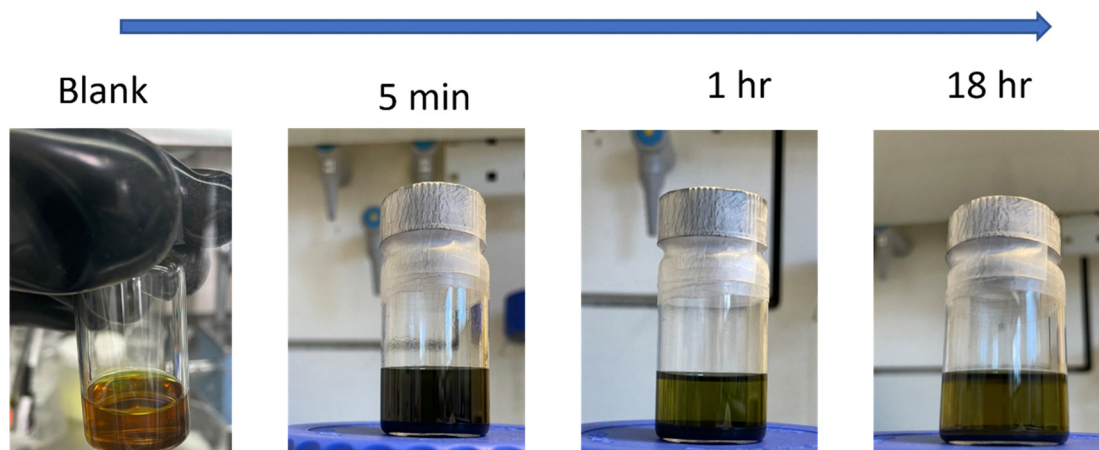**Fig. 7** Static lithium polysulfide adsorption tests of Li_2S_6 solutions after adding $Li_2S/C/SnS_2$ (5%).

polysulfide shuttling. Carbon provides a conductive network that facilitates electron transport, while SnS_2 acts as a polar host, chemically adsorbing polysulfides and promoting their conversion and reducing capacity loss. This synergy leads to higher sulfur utilization, improved cycling stability, and enhanced rate performance in Li–S batteries. The $Li_2S/C/SnS_2$ (5%) with a carbon content of 20% shows relatively high capacity and capacity retention. According to the literature, SnS_2 enhances the performance of Li–S batteries by suppressing the shuttle effect and catalyzing redox reactions. SnS_2 provides a polar surface that strongly adsorbs polysulfides, reducing their dissolution and diffusion, which mitigates capacity fading.[42,43] However, the composite containing a relatively high concentration of SnS_2 (12%) did not perform as well. This is due to the decrease in carbon concentration from 25 wt% to 12.5 wt% as the SnS_2 content increased with a constant amount of Li_2S. This suggests that improving the performance of the Li_2S cathode for an efficient Li–S battery requires the presence of both carbon and the SnS_2 additive.

Conclusions

We have prepared three types of $Li_2S/C/SnS_2$ composites with different weight ratios of carbon and SnS_2 while keeping the weight of the active material Li_2S constant at 75%. High energy mechanical milling, which is a very convenient and highly scalable method, was used to synthesize the composites. After characterizing the composites physically and chemically, we studied their electrochemical performance as a cathode in the lithium–sulfur system. The $Li_2S/C/SnS_2$ composites with different contents of carbon and SnS_2 all show low activation overpotentials compared to pure Li_2S when used as cathode materials for Li–S batteries. *Via* the synergistic effect of carbon and SnS_2, the $Li_2S/C/SnS_2$ (5%) composite with 20% carbon content exhibits a high utilization rate of the active material and strong retention of lithium polysulfides, resulting in good cycling stability and high discharge capacity. With a high mass ratio (75%) of the active material (Li_2S), and optimized contents of carbon and SnS_2, Li_2S-based composites can be paired with lithium-free anodes such as graphite and Si, thereby circumventing the safety issues associated with the use of metallic lithium. Furthermore, the results and characterization provided here offer a better understanding of Li_2S cathodes and pave the way for designing improved electrodes in the future.

Author contributions

Conceptualisation: Irshad Mohammad and Damian Cupid; methodology: Irshad Mohammad, Yuri Surace and Akzhan Bekzhanov; investigation: Irshad Mohammad and Akzhan Bekzhanov; writing – original draft preparation: Irshad Mohammad; writing – review and editing: Damian Cupic, Yuri Surace and Akzhan Bekzhanov. All authors have read and agreed to the published version of the manuscript.

Conflicts of interest

The authors declare that they have no known competing financial interests or personal relationships that could have appeared to influence the work reported in this paper.

Data availability

All data analysed in this study are included in this main article and its SI. Supplementary information: Table S1 Percentage of individual components in the Li_2S composites. Observed and calculated XRD patterns of as ball-milled $Li_2S/C/SnS_2$ composites. EDX images and mapping of $Li_2S/C/SnS_2$ (5%) cathode. SEM image of the as-received Li_2S powder. Cycling performance for pure Li_2S electrode based Li–S cells. Fitting parameter values for Nyquist plots obtained at 25 °C for Li_2S/C, $Li_2S/C/SnS_2$ (5%), and $Li_2S/C/SnS_2$ (12.5%) electrode-based cells. Rate performance of $Li_2S/C/SnS_2$ (5%) electrode at a current rate range of 1C to 5C. Fitting parameter values for Nyquist plots obtained at 25 °C for $Li_2S/C/SnS_2$ (5%) cell before and after 200 cycling. Long cycling up to 200 cycles for $Li_2S/C/SnS_2$ (5%) and Li_2S/C after the EIS measurement at OCV. See DOI: **https://doi.org/10.1039/d5ya00206k**.

Any other data related to this study are available from the corresponding author upon reasonable request.

Acknowledgements

References

1 M. Armand and J.-M. Tarascon, Building better batteries, *Nature*, 2008, **451**(7179), 652–657, DOI: **10.1038/451652a**.

2 S. Zhang, *et al.*, A novel strategy to significantly enhance the initial voltage and suppress voltage fading of a Li- and Mn-rich layered oxide cathode material for lithium-ion batteries, *J. Mater. Chem. A*, 2018, **6**(8), 3610–3624, DOI: **10.1039/C7TA10887G**.

3 A. Manthiram, Y. Fu and Y.-S. Su, Challenges and Prospects of Lithium–Sulfur Batteries, *Acc. Chem. Res.*, 2013, **46**(5), 1125–1134, DOI: **10.1021/ar300179v**.

4 A. Manthiram, Y. Fu, S.-H. Chung, C. Zu and Y.-S. Su, Rechargeable Lithium–Sulfur Batteries, *Chem. Rev.*, 2014, **114**(23), 11751–11787, DOI: **10.1021/cr500062v**.

5 Y. Liu, *et al.*, Electrolyte solutions design for lithium-sulfur batteries, *Joule*, 2021, **5**(9), 2323–2364, DOI: **10.1016/j.joule.2021.06.009**.

6 T. Wang, G. Cui, Y. Zhao, A. Nurpeissova and Z. Bakenov, Porous carbon nanotubes microspheres decorated with strong catalyst cobalt nanoparticles as an effective sulfur host for lithium-sulfur battery, *J. Alloys Compd.*, 2021, **853**, 157268, DOI: **10.1016/j.jallcom.2020.157268**.

7 Z.-D. Huang, et al., Sulfur in Mesoporous Tungsten Nitride Foam Blocks: A Rational Lithium Polysulfide Confinement Experimental Design Strategy Augmented by Theoretical Predictions, ACS Appl. Mater. Interfaces, 2019, 11(22), 20013–20021, DOI: 10.1021/acsami.9b04246.

8 M. Yan, et al., 3D Ferroconcrete-Like Aminated Carbon Nanotubes Network Anchoring Sulfur for Advanced Lithium–Sulfur Battery, Adv. Energy Mater., 2018, 8(25), 1801066, DOI: 10.1002/aenm.201801066.

9 S.-F. Ng, M. Y. L. Lau and W.-J. Ong, Lithium–Sulfur Battery Cathode Design: Tailoring Metal-Based Nanostructures for Robust Polysulfide Adsorption and Catalytic Conversion, Adv. Mater., 2021, 33(50), 2008654, DOI: 10.1002/adma.202008654.

10 J. Lee and W. Choi, Surface Modification of Sulfur Cathodes with PEDOT:PSS Conducting Polymer in Lithium-Sulfur Batteries, J. Electrochem. Soc., 2015, 162(6), A935, DOI: 10.1149/2.0651506jes.

11 W. Chen, et al., Designing Safe Electrolyte Systems for a High-Stability Lithium–Sulfur Battery, Adv. Energy Mater., 2018, 8(10), 1702348, DOI: 10.1002/aenm.201702348.

12 X. Xiong, et al., Methods to Improve Lithium Metal Anode for Li-S Batteries, Front. Chem., 2019, 7, 827, accessed: Mar. 04, 2023. [Online]. Available: https://www.frontiersin.org/articles/10.3389/fchem.2019.00827.

13 I. Mohammad, L. D. J. Barter, V. Stolojan, C. Crean and R. C. T. Slade, Electrospun polar-nanofiber PVDF separator for lithium–sulfur batteries with enhanced charge storage capacity and cycling durability, Energy Adv., 2024, 3(3), 625–635, DOI: 10.1039/D3YA00392B.

14 J. Li, et al., Functionally Modified Polyolefin-Based Separators for Lithium-Sulfur Batteries: Progress and Prospects, Front. Energy Res., 2020, 8, 593640, accessed: Mar. 04, 2023. [Online]. Available:.

15 I. Mohammad, L. D. J. Barter, C. Crean and R. C. T. Slade, Addition of a Polar, Porous Phase-Inversion-PVDF Membrane to Lithium–Sulfur Cells (LSBs) Already with a Microporous Polypropylene Separator Enhances the Battery Performance, Batteries, 2024, 10(8), 8, DOI: 10.3390/batteries10080293.

16 C. Zhou, et al., An ultrathin and crack-free metal-organic framework film for effective polysulfide inhibition in lithium–sulfur batteries, Interdiscip. Mater., 2024, 3(2), 306–315, DOI: 10.1002/idm2.12143.

17 C. Dong, et al., Engineering d-p Orbital Hybridization with P, S Co-Coordination Asymmetric Configuration of Single Atoms Toward High-Rate and Long-Cycling Lithium–Sulfur Battery, Adv. Mater., 2024, 36(38), 2407070, DOI: 10.1002/adma.202407070.

18 Y. He, et al., Simultaneously Inhibiting Lithium Dendrites Growth and Polysulfides Shuttle by a Flexible MOF-Based Membrane in Li–S Batteries, Adv. Energy Mater., 2018, 8(34), 1802130, DOI: 10.1002/aenm.201802130.

19 L. Li, et al., Self-heating–induced healing of lithium dendrites, Science, 2018, 359(6383), 1513–1516, DOI: 10.1126/science.aap8787.

20 Q. Pang, A. Shyamsunder, B. Narayanan, C. Y. Kwok, L. A. Curtiss and L. F. Nazar, Tuning the electrolyte network structure to invoke quasi-solid state sulfur conversion and suppress lithium dendrite formation in Li–S batteries, Nat. Energy, 2018, 3(9), 783–791, DOI: 10.1038/s41560-018-0214-0.

21 T. Seita, et al., Graphite–Lithium Sulfide Battery with a Single-Phase Sparingly Solvating Electrolyte, ACS Energy Lett., 2020, 5(1), 1–7, DOI: 10.1021/acsenergylett.9b02347.

22 Z. Hao, et al., Advanced Li2S/Si Full Battery Enabled by TiN Polysulfide Immobilizer, Small, 2019, 15(50), 1902377, DOI: 10.1002/smll.201902377.

23 Y. Chen, S. Lu, Y. Li, W. Qin and X. Wu, A high-performance Li2S/MnO2 rechargeable battery, Mater. Lett., 2019, 248, 157–160, DOI: 10.1016/j.matlet.2019.04.018.

24 M. Liu, D. Zhou, H. R. Jiang, Y. X. Ren, F. Y. Kang and T. S. Zhao, A highly-safe lithium-ion sulfur polymer battery with SnO2 anode and acrylate-based gel polymer electrolyte, Nano Energy, 2016, 28, 97–105, DOI: 10.1016/j.nanoen.2016.08.033.

25 D. S. Wu, et al., A novel battery scheme: Coupling nanostructured phosphorus anodes with lithium sulfide cathodes, Nano Res., 2020, 13(5), 1383–1388, DOI: 10.1007/s12274-020-2645-8.

26 Y. Yang, G. Zheng, S. Misra, J. Nelson, M. F. Toney and Y. Cui, High-Capacity Micrometer-Sized Li2S Particles as Cathode Materials for Advanced Rechargeable Lithium-Ion Batteries, J. Am. Chem. Soc., 2012, 134(37), 15387–15394, DOI: 10.1021/ja3052206.

27 C. Chen, D. Li, L. Gao, P. P. R. M. L. Harks, R.-A. Eichel and P. H. L. Notten, Carbon-coated core–shell Li2S@C nanocomposites as high performance cathode materials for lithium–sulfur batteries, J. Mater. Chem. A, 2017, 5(4), 1428–1433, DOI: 10.1039/C6TA09146F.

28 G. Gao, X. Yang, J. Bi, W. Guan, Z. Du and W. Ai, Advanced engineering strategies for Li2S cathodes in lithium–sulfur batteries, J. Mater. Chem. A, 2023, 11(48), 26318–26339, DOI: 10.1039/D3TA06057H.

29 Y. Ji, et al., MoC nanoparticles decorated carbon nanofibers loaded with Li2S as high-performance lithium sulfur battery cathodes, Appl. Surf. Sci., 2025, 679, 161263, DOI: 10.1016/j.apsusc.2024.161263.

30 K. Cai, M.-K. Song, E. J. Cairns and Y. Zhang, Nanostructured Li2S–C Composites as Cathode Material for High-Energy Lithium/Sulfur Batteries, Nano Lett., 2012, 12(12), 6474–6479, DOI: 10.1021/nl303965a.

31 H. Gamo, K. Hikima and A. Matsuda, Transition-Metal Sulfides for High-Performance Lithium Sulfide Cathodes in All-Solid-State Lithium–Sulfur Batteries, ACS Omega, 2023, 8(48), 45557–45565, DOI: 10.1021/acsomega.3c05635.

32 G. Zhou, et al., Catalytic oxidation of Li2S on the surface of metal sulfides for Li−S batteries, Proc. Natl. Acad. Sci. U. S. A., 2017, 114(5), 840–845, DOI: 10.1073/pnas.1615837114.

33 W. Jun, C. Bing, L. Qingqing, H. Ailin, L. Xiaoying and J. Qi, Preparing a composite including SnS2, carbon nanotubes and S and using as cathode material of lithium-sulfur

battery, *Scr. Mater.*, 2020, **177**, 208–213, DOI: **10.1016/j.scriptamat.2019.10.038**.

34 K. Sun, *et al.*, Interaction of FeS2 and Sulfur in Li-S Battery System, *J. Electrochem. Soc.*, 2016, **164**(1), A6039, DOI: **10.1149/2.0041701jes**.

35 A. Bekzhanov, N. Daniyeva, Q. Jiang, Y. Surace, F. Kleitz and D. Cupid, Hydrothermally Synthesized SnS$_2$ Anode Materials with Selectively Tuned Crystallinity, *Small Science*, 2025, **5**(5), 2400516, DOI: **10.1002/smsc.202400516**.

36 A. Glibo, N. Eshraghi, Y. Surace, A. Mautner, H. Flandorfer and D. M. Cupid, Comparative study of electrochemical properties of SnS and SnS$_2$ as anode materials in lithium-ion batteries, *Electrochim. Acta*, 2023, **441**, 141725, DOI: **10.1016/j.electacta.2022.141725**.

37 D. M. Cupid, *et al.*, Understanding and modelling the thermodynamics and electrochemistry of lithiation of tin (IV) sulfide as an anode active material for lithium ion batteries, *Electrochim. Acta*, 2021, **375**, 137936, DOI: **10.1016/j.electacta.2021.137936**.

38 H. El-Shinawi, E. J. Cussen and S. A. Corr, A facile synthetic approach to nanostructured Li2S cathodes for rechargeable

solid-state Li–S batteries, *Nanoscale*, 2019, **11**(41), 19297–19300, DOI: **10.1039/C9NR06239D**.

39 N. Yahalom, *et al.*, Durable Lithium–Sulfur Batteries Based on a Composite Carbon Nanotube Cathode, *ACS Appl. Energy Mater.*, 2023, **6**(9), 4511–4519, DOI: **10.1021/acsaem.3c00487**.

40 J. Yan, X. Liu and B. Li, Capacity Fade Analysis of Sulfur Cathodes in Lithium–Sulfur Batteries, *Adv. Sci.*, 2016, **3**(12), 1600101, DOI: **10.1002/advs.201600101**.

41 X. Tao, *et al.*, Strong Sulfur Binding with Conducting Magnéli-Phase TinO2n–1 Nanomaterials for Improving Lithium–Sulfur Batteries, *Nano Lett.*, 2014, **14**(9), 5288–5294, DOI: **10.1021/nl502331f**.

42 C. Wei, *et al.*, Advanced lithium–sulfur batteries enabled by a SnS$_2$-Hollow carbon nanofibers Flexible Electrocatalytic Membrane, *Carbon*, 2021, **184**, 1–11, DOI: **10.1016/j.carbon.2021.08.004**.

43 H. Liu, *et al.*, Hollow cubic ZnS–SnS$_2$ heterostructures as sulfur hosts to enhance chemisorption and catalytic conversion of polysulfides for lithium sulfur batteries, *J. Electroanal. Chem.*, 2023, **932**, 117252, DOI: **10.1016/j.jelechem.2023.117252**.